光学学报

InGaAs自适应阱簇复合结构的偏振双峰辐射机制及能带特征

于庆南[1*]，李可[1]，王新宇[1]，吴坚[2]，张建伟[3]，刘子键[1]，邢佳童[1]，廖玲[1]，季慧娴[1]，王青[1]，李晖[1]

[1]无锡学院电子信息工程学院，江苏 无锡 214105；

[2]北京航空航天大学物理学院，北京 100191；

[3]中国科学院长春光学精密机械与物理研究所，吉林 长春 130033

摘要 研究一种基于富铟团簇(IRC)效应的新型高应变InGaAs/GaAs自适应阱簇复合(WCC)量子结构，该结构具有比较灵活的能带调控能力，可产生一种特殊的偏振双峰光谱。为探究该WCC结构的偏振双峰辐射机制及能带特征，利用IRC效应生长获得了自适应WCC结构，并测量了该新型结构的偏振光致发光(PL)光谱，在横向电场(TE)和横向磁场(TM)模式下，PL光谱皆显示出特殊的双峰结构。这主要是铟原子的自适应迁移导致有源层同时存在铟组分正常和铟组分降低的$In_xGa_{1-x}As$材料所致。根据半导体激光器的跃迁矩阵元理论和PL光谱的双峰能量间距，阐明不同偏振模式下的光谱双峰与多组分$In_xGa_{1-x}As$材料的对应辐射机制，同时确定该WCC结构的混合能带特征。该研究内容对IRC效应和新型WCC发光结构的发展和应用具有重要研究意义。

关键词 半导体激光器；InGaAs/GaAs；富铟团簇；偏振双峰光谱；混合能带

中图分类号 O432 **文献标志码** A **DOI**：10.3788/AOS222184

1 引 言

常规的InGaAs/GaAs应变量子阱具有固定的铟含量和单一的应变类型[1-4]，已经广泛应用于半导体光放大器、光纤通信、生物医学等众多领域[5-7]。在生长常规的高应变InGaAs量子阱时，富铟团簇(IRC)效应通常被作为一种生长缺陷来规避[8-10]，因此忽略了其特殊的光学特性。所谓IRC效应，即在生长高应变InGaAs/GaAs量子结构时，为了释放InGaAs材料中积累的高应变，铟原子会沿着材料生长方向自动向上迁移，并在InGaAs材料表面堆积，形成三维团簇(IRC)。近几年，本课题组基于IRC效应，生长获得了一种新型非对称InGaAs自适应阱簇复合(WCC)量子限制结构，该WCC有源层包含了大量不同铟含量的$In_xGa_{1-x}As$激活区以及混合应变类型，且偏振光致发光(PL)谱具有明显的双峰结构。本课题组通过测量WCC样品两端的PL光谱，计算并分析了其超宽的增益特性，有望实现100 nm的超宽调谐激光器[11]。此外，利用高斯拟合探究了PL光谱的构成，分析并实现了在单一WCC结构上的双波长的同步激射[12]。同时，该WCC结构中几乎等大的横向电场(TE)和横向磁场(TM)偏振增益对实现偏振独立光放大器也具有重要的研究价值[13]。由于该WCC结构是基于IRC效应形成的，该效应会引起铟原子的自适应迁移，进而导致在单一InGaAs有源层内同时产生铟组分正常的和铟组分降低的$In_xGa_{1-x}As$区域以及张压应变同时存在的混合能带类型，以上复杂特征导致偏振双峰与多组分$In_xGa_{1-x}As$材料的对应辐射机制尚不清晰。因此，探究清楚InGaAs自适应WCC结构的偏振双峰辐射机制和混合能带特征对研究和评估新型WCC半导体激光器具有重要意义[14-15]。

本文首先利用IRC效应生长获得了InGaAs自适应WCC量子结构，并在室温下测量了该结构在TE和TM模式下的PL光谱，其皆呈现出明显的两个谱峰。根据半导体激光器的跃迁矩阵元理论，阐明了偏振光谱双峰与多组分$In_xGa_{1-x}As$材料的对应辐射机制，同时获得了包含第一导带(C_1)以及第一重空穴带(HH_1)和轻空穴带(LH_1)的混合能带结构。

2 $In_xGa_{1-x}As$自适应WCC量子结构

利用金属有机化学气相沉积系统(MOCVD)，在

收稿日期：2022-12-29；**修回日期**：2023-01-28；**录用日期**：2023-02-09；**网络首发日期**：2023-03-09

基金项目：国家自然科学基金(62204172)、江苏省双创博士(JSSCBS20210870，JSSCBS20210868)、江苏省高等学校自然科学基金(22KJB140016)、江苏省高等学校自然科学研究面上项目(17KJB510037)、南京信息工程大学滨江学院引进人才启动基金(550221009，550221036)

通信作者：*yuqingnan1@126.com

未掺杂的GaAs(001)衬底上生长获得了基于IRC效应的InGaAs自适应WCC量子结构。形成IRC的基本原理是在生长高应变$In_xGa_{1-x}As$/GaAs量子结构时，为了释放$In_xGa_{1-x}As$量子阱中逐渐积累的高应变，铟原子会沿着材料生长方向自动向上迁移，并在$In_xGa_{1-x}As$材料表面堆积，形成富铟团簇[16-17]。为了生长获得InGaAs自适应WCC量子结构，本文设计$In_{0.17}Ga_{0.83}As$/GaAs/$GaAsP_{0.08}$材料体系为有源区，其中$GaAsP_{0.08}$势垒层厚8 nm，用来吸收泵浦光；$In_{0.17}Ga_{0.83}As$势阱的层厚被设计为10 nm；由于WCC量子结构的形成主要取决于$In_{0.17}Ga_{0.83}As$材料内部的应变积累，为了更好地标定和补偿$In_{0.17}Ga_{0.83}As$材料内部的应变，在势阱和势垒之间增加了2 nm厚的GaAs应变补偿(SC)层。InGaAs自适应WCC量子限制结构如图1(a)所示。其中10 nm的厚度设计是为了获得足够的应变积累，有利于IRC的产生。只有当$In_xGa_{1-x}As$层的生长厚度超过若干个单分子层后，为释放较大晶格失配引起的应变积累，铟原子才会迁移到InGaAs层表面堆积并形成IRC，同时会在有源区产生铟组分正常的$In_{0.17}Ga_{0.83}As$材料和铟组分降低的$In_xGa_{1-x}As$区域，形成原理如图1(b)所示。为确保生长的WCC结构中包含IRC，本文使用原子力显微镜(AFM；XE100，Park Systems Instrument公司)测量获得了InGaAs的上表面形貌，结果如图1(a)中的插图所示。原子力照片中展现了大量不规则的三维团簇形貌，即IRC，说明该结构产生了IRC效应。

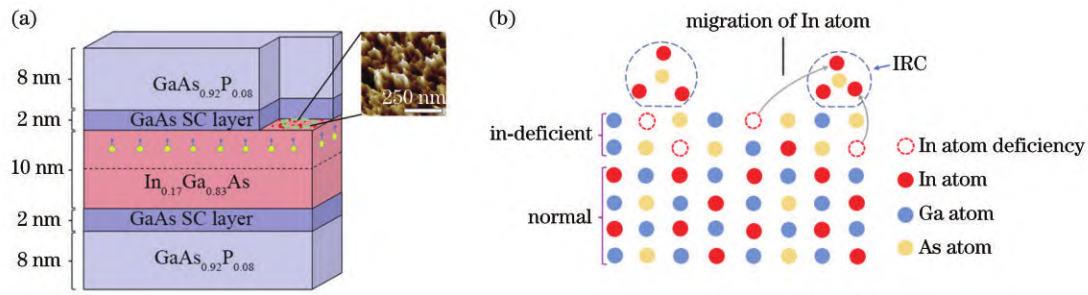

图1　InGaAs自适应WCC量子结构及IRC形成机制。(a) WCC量子结构及IRC形貌；(b) IRC形成原理

Fig. 1　InGaAs self-fit WCC quantum structure and formation mechanism of IRC. (a) WCC quantum structure and IRC topography; (b) formation principle of IRC

3　偏振双峰光谱的实验测量

为了探究InGaAs/GaAs WCC量子结构的偏振双峰辐射机制，在不同的载流子注入浓度下(N=3.0×10^{17}，3.6×10^{17}，3.9×10^{17}，4.5×10^{17} cm^{-3})，利用线性偏振片分别测量了该WCC结构的TE和TM偏振PL光谱，测量原理如图2(a)所示。为避免端面反射对光谱峰值的影响，该WCC结构两端都进行了增透处理，透过率T=99.99%。波长为808 nm的光纤耦合激光器作为泵浦源，线性偏振片和两个焦距为10 cm的平凸透镜用于收集不同偏振模式下的PL谱，测量结果如图2(b)所示。

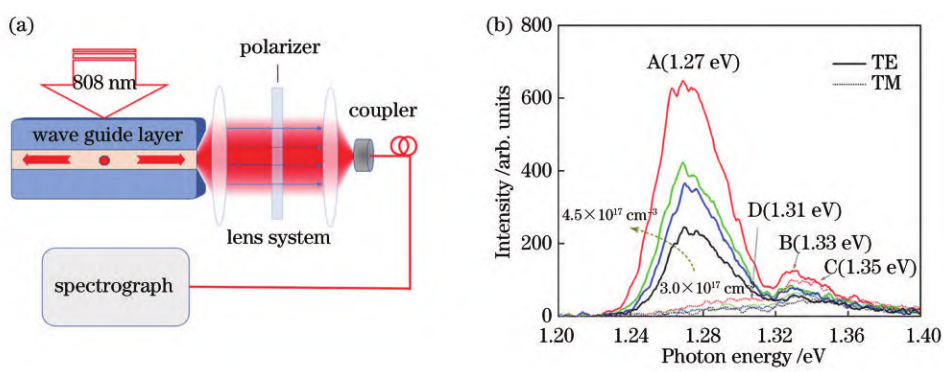

图2　PL光谱的测量原理及光谱曲线。(a) PL光谱的测量原理；(b) TE和TM偏振模式下的PL光谱

Fig. 2　PL spectral measurement principle and spectral curves. (a) PL spectral measurement principle; (b) PL spectra in the TE and TM polarizations

图2(b)中TE和TM偏振PL光谱皆呈现出特殊的双峰特征，即每条谱线都具有明显的两个峰，这里分别用A、B和C、D标记两种偏振模式下的峰值点，对应的光子能量分别为1.27 eV、1.33 eV和1.35 eV、1.31 eV，峰谷能量约为1.317 eV。该双峰特征产生的原因是在$In_xGa_{1-x}As$/GaAs材料生长过程中发生了IRC效应，铟原子的自适应迁移导致正常$In_{0.17}Ga_{0.83}As$材料中铟含量降低，形成铟组分降低的$In_xGa_{1-x}As$区

域。由于该低铟区域带隙较宽，PL 谱峰向短波方向偏移。该低铟区域与正常的 $In_{0.17}Ga_{0.83}As$ 材料共同产生了图 2 中的双峰光谱。由于该 WCC 结构是基于 IRC 效应产生的，铟原子因自适应迁移会在顶部堆积，产生 IRC 以及铟组分降低的有源区。富铟团簇的大小和分布具有一定的随机性，会导致有源区的铟含量产生一定起伏，进而会影响光谱的细节特征，但总体的双峰特征不变[11-12]。为探究 TE 和 TM 偏振光谱双峰与多组分 $In_xGa_{1-x}As$ 区域的对应辐射机制及能带特征，本文将利用跃迁矩阵元理论和 Model-Solid 理论进行分析和验证。

4　分析与讨论

4.1　WCC 结构的能带特征

根据 Model-Solid 理论，当载流子注入浓度较低时，电子主要占据带边能级，光谱峰值对应的光子能量主要取决于导带 C_1 到价带之间的能量间隔。根据本课题组的前期研究，该非对称 WCC 结构主要包括两种不同铟含量的 $In_xGa_{1-x}As$ 材料，即铟组分降低的 $In_{0.12}Ga_{0.88}As$ 层和铟组分正常的 $In_{0.17}Ga_{0.83}As$ 材料[13]。由于铟原子的自适应迁移是在 $In_{0.17}Ga_{0.83}As$ 生长到若干个单分子层后发生的，因此，低铟的 $In_{0.12}Ga_{0.88}As$ 材料位于正常的 $In_{0.17}Ga_{0.83}As$ 层上表面，如图 1 所示。为确定该非对称量子结构的应变类型，$In_xGa_{1-x}As$ 材料的晶格常数 $a(x)$[18] 可表示为

$$a(x)=6.0583-0.405(1-x), \tag{1}$$

式中：x 表示 $In_xGa_{1-x}As$ 材料的铟含量。根据式(1)求得 GaAs、$In_{0.17}Ga_{0.83}As$ 和 $In_{0.12}Ga_{0.88}As$ 的晶格常数分别为 5.65325 Å、5.72215 Å 和 5.7019 Å(1 Å=10^{-10} m)，其晶格失配情况如图 3(a)所示。经计算可知，生长在 GaAs 上的 $In_{0.17}Ga_{0.83}As$ 材料和生长在 $In_{0.17}Ga_{0.83}As$ 上的 $In_{0.12}Ga_{0.88}As$ 材料对应的应变量分别为 0.012 和 −0.004。因此，这种特殊的自适应 WCC 量子限制结构产生了一种特殊的混合应变类型，即在正常的 $In_{0.17}Ga_{0.83}As$ 层中产生压应变，其重空穴带 HH_1 位于轻空穴带 LH_1 上方；在低铟的 $In_{0.12}Ga_{0.88}As$ 层中产生张应变，其轻空穴带 LH_1 位于重空穴带 HH_1 上方。混合能带结构如图 3(b)所示。

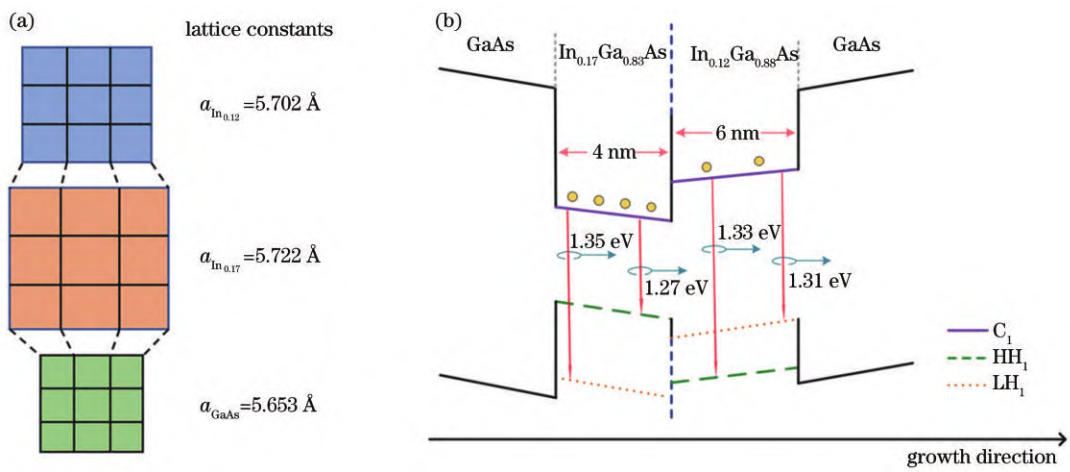

图 3　$In_xGa_{1-x}As$/GaAs 材料系统的晶格失配及 InGaAs 自适应 WCC 量子结构的能带特征。(a) $In_{0.12}Ga_{0.88}As$、$In_{0.17}Ga_{0.83}As$ 与 GaAs 材料的晶格失配；(b)能带特性

Fig. 3　Lattice mismatch of $In_xGa_{1-x}As$/GaAs material system and energy band characteristics of InGaAs self-fit WCC quantum structure. (a) Lattice mismatch of $In_{0.12}G_{0.88}As$, $In_{0.17}Ga_{0.83}As$, and GaAs; (b) energy band characteristic

4.2　偏振双峰的对应辐射机制

为探究偏振光谱的双峰与混合能带的对应辐射机制，根据半导体激光器的跃迁矩阵元理论进行如下分析。当电子在导带 C_1 和重空穴 HH_1 能级之间跃迁时，TE 偏振的跃迁矩阵元值为 $|\boldsymbol{M}|^2_{TE}=|\boldsymbol{M}|^2/2$，而 TM 偏振的跃迁矩阵元 $|\boldsymbol{M}|^2_{TM}=0$，此时产生 TE 偏振的电子跃迁速率大于 TM 偏振的电子跃迁速率，TE 偏振的光谱强度会明显大于 TM 偏振光谱；而当电子从导带 C_1 跃迁到轻空穴 LH_1 时，TE 偏振跃迁矩阵元 $|\boldsymbol{M}|^2_{TE}=|\boldsymbol{M}|^2/6$，而 TM 偏振跃迁矩阵元 $|\boldsymbol{M}|^2_{TM}=2|\boldsymbol{M}|^2/3$，TM 偏振的光谱强度呈现出超过 TE 偏振光谱的趋势，其中的 $|\boldsymbol{M}|^2$ 是一个常量，为材料的动量矩阵元[19]。因此，TE 偏振光谱主要由 C_1 和重空穴 HH_1 之间的电子-空穴复合决定，TM 偏振光谱主要由 C_1 与轻空穴 LH_1 之间的电子-空穴复合决定，TE 和 TM 光谱峰值之间的能量间隔对应于 HH_1 和 LH_1 之间的能量间距。

根据跃迁矩阵元理论，在压应变的 $In_{0.17}Ga_{0.83}As$ 材料中，其重空穴带 HH_1 位于轻空穴带 LH_1 上方，该材料辐射的 TE 偏振的光子能量要小于 TM 偏振光谱。而在具有张应变的 $In_{0.12}Ga_{0.88}As$ 材料中，其轻空穴带 LH_1 位于重空穴带 HH_1 上方，TM 光谱对应的光子能量要小于 TE 光谱。根据跃迁矩阵元的分析，并结合图 2(b)中的不同偏振模式下的双峰可以判断：TE 和 TM

光谱曲线中的主峰A(1.27 eV)和C(1.35 eV)主要是压应变$In_{0.17}Ga_{0.83}As$材料发生辐射产生的;图2(b)中TE和TM曲线中的次峰B(1.33 eV)和D(1.31 eV)主要是张应变的$In_{0.12}Ga_{0.88}As$材料发生辐射产生的。偏振双峰的对应辐射机制及混合能带特征如图3(b)所示。另外,图中正常的$In_{0.17}Ga_{0.83}As$材料厚度为4 nm,这一结论是基于本课题组前期对WCC结构进行逐点扫描测量得到的实验结果[20]。

通过图3(b)可知:对于压应变$In_{0.17}Ga_{0.83}As$材料,其重空穴和轻空穴的能量间距为0.08 eV;对于张应变$In_{0.12}Ga_{0.88}As$材料,重轻空穴的能量间隔为0.02 eV。为验证WCC结构的能带特性及偏振双峰对应辐射机制的准确性,根据Model-Solid理论分别计算得到了压应变$In_{0.17}Ga_{0.83}As$材料和张应变$In_{0.12}Ga_{0.88}As$材料中LH_1和HH_1之间的能量间隔[21-22],计算公式为

$$\Delta E_{HH}(x,y)=2a_v\left(1-\frac{C_{12}}{C_{11}}\right)\varepsilon+|\boldsymbol{b}|\left(1+2\frac{C_{12}}{C_{11}}\right)\varepsilon, \tag{2}$$

$$\Delta E_{LH}(x,y)=2a_v\left(1-\frac{C_{12}}{C_{11}}\right)\varepsilon-|\boldsymbol{b}|\left(1+2\frac{C_{12}}{C_{11}}\right)\varepsilon, \tag{3}$$

式中:ΔE_{HH}和ΔE_{LH}分别代表应变引起的重空穴和轻空穴的能带偏移量;a_v表示半导体材料中价带的形变势;ε表示应变;C_{11}和C_{12}代表弹性常量;$\boldsymbol{b}$代表柏氏向量。根据式(2)和式(3)可知,晶格失配引起的应变会导致HH_1和LH_1发生分离和偏移。在$In_{0.17}Ga_{0.83}As$材料中,HH_1和LH_1的能带偏移分别为$\Delta E_{HH}=0.025$ eV和$\Delta E_{LH}=-0.0544$ eV,因此HH_1和LH_1之间的能量间隔为$\Delta E_{0.17}=0.079$ eV。对于$In_{0.12}Ga_{0.88}As$材料,HH_1和LH_1的能带偏移分别为$\Delta E_{HH}=-0.0073$ eV和$\Delta E_{LH}=0.0161$ eV,因此HH_1和LH_1之间的能量间隔为$\Delta E_{0.12}=0.023$ eV。理论结果与图3所示的实验数据基本一致。这表明了该非对称InGaAs自适应WCC量子结构中能带特征及偏振双峰对应辐射机制的准确性。

5 结 论

基于生长高应变InGaAs量子阱中的富铟团簇效应,生长获得了一种特殊的非对称自适应WCC结构,测量了该新型结构TE和TM模式下的光致发光光谱,光谱皆呈现出特殊的双峰特征。根据半导体激光器的跃迁矩阵元理论,结合偏振双峰的能量间距,阐明了偏振双峰与多组分$In_xGa_{1-x}As$材料的对应辐射机制,同时确定了该非对称结构的能带具有压/张应变同时存在的混合应变特征。该研究结果对分析InGaAs非对称WCC结构具有重要意义。

参 考 文 献

[1] 何天将, 井红旗, 朱凌妮, 等. 对915 nm InGaAsP/GaAsP初次外延片量子阱混杂的研究[J]. 光学学报, 2022, 42(1): 0114003.
He T J, Jing H Q, Zhu L N, et al. Quantum well intermixing of 915 nm InGaAsP/GaAsP primary epitaxial wafers[J]. Acta Optica Sinica, 2022, 42(1): 0114003.

[2] 王予晓, 朱凌妮, 仲莉, 等. Si_xN_y沉积参数对量子阱混杂效果的影响[J]. 光学学报, 2022, 42(10): 1031003.
Wang Y X, Zhu L N, Zhong L, et al. Influence of Si_xN_y deposition parameters on intermixing of quantum wells[J]. Acta Optica Sinica, 2022, 42(10): 1031003.

[3] Li Y, Yuan W F, Li K, et al. InGaAs/InAlAs SAGCMCT avalanche photodiode with high linearity and wide dynamic range [J]. Chinese Optics Letters, 2022, 20(2): 022503.

[4] 崔星宇, 林逢源, 张志宏, 等. 低噪声InGaAs/InP雪崩光电二极管的模拟分析[J]. 中国激光, 2021, 48(17): 1701001.
Cui X Y, Lin F Y, Zhang Z H, et al. Simulation analysis of low-noise InGaAs/InP avalanche photodiodes[J]. Chinese Journal of Lasers, 2021, 48(17): 1701001.

[5] 吴坚, 王玉红, 郜含旭, 等. 低维铟基阱-点复合量子结构及光学性能和应用前景[J]. 中国激光, 2022, 49(19): 1901002.
Wu J, Wang Y H, Tai H X, et al. Low-dimensional indium-based well-dot composite quantum structures and their optical properties and application prospects[J]. Chinese Journal of Lasers, 2022, 49(19): 1901002.

[6] 罗妍, 郝永芹, 邹永刚. 应用于VCSEL的GaAs/AlO_x高折射率对比度亚波长光栅反射镜的设计和制备[J]. 光学学报, 2023, 43(1): 0105002.
Luo Y, Hao Y Q, Zou Y G. Design and fabrication of GaAs/AlO_x high-index-contrast sub-wavelength grating reflector for VCSEL[J]. Acta Optica Sinica, 2023, 43(1): 0105002.

[7] 荣敏敏, 张益军, 李诗曼, 等. 基于扫描聚焦XPS技术的InGaAs表面清洁研究[J]. 光学学报, 2021, 41(5): 0516004.
Rong M M, Zhang Y J, Li S M, et al. InGaAs surface cleaning based on scanning focused XPS technique[J]. Acta Optica Sinica, 2021, 41(5): 0516004.

[8] Schlenker D, Miyamoto T, Chen Z, et al. Growth of highly strained GaInAs/GaAs quantum wells for 1.2 μm wavelength lasers[J]. Journal of Crystal Growth, 2000, 209(1): 27-36.

[9] Ma S J, Wang Y, Sodabanlu H, et al. Effect of hetero-interfaces on *in situ* wafer curvature behavior in InGaAs/GaAsP strain-balanced MQWs[J]. Journal of Crystal Growth, 2012, 352 (1): 245-248.

[10] Muraki K, Fukatsu S, Shiraki Y, et al. Surface segregation of in atoms during molecular beam epitaxy and its influence on the energy levels in InGaAs/GaAs quantum wells[J]. Applied Physics Letters, 1992, 61(5): 557-559.

[11] Yu Q N, Li X, Jia Y, et al. InGaAs-based well - island composite quantum-confined structure with superwide and uniform gain distribution for great enhancement of semiconductor laser performance[J]. ACS Photonics, 2018, 5(12): 4896-4902.

[12] Yu Q N, Zheng M, Tai H X, et al. Quantum confined indium-rich cluster lasers with polarized dual-wavelength output[J]. ACS Photonics, 2019, 6(8): 1990-1995.

[13] Zheng M, Yu Q N, Tai H X, et al. Experimental investigation of spontaneous emission characteristics of InGaAs-based indium-rich cluster-induced special quantum structure[J]. Chinese Optics Letters, 2020, 18(5): 051403.

[14] Duan L H, Fang L, Zhang J, et al. Fabrication and characteristics of high speed InGaAs/GaAs quantum-wells superluminescent diode emitting at 1053 nm[J]. Semiconductor Science and Technology, 2014, 29(5): 055004.

[15] Jung A, Taboada A G, Stumpf W, et al. Heterointegration of InGaAs/GaAs quantum wells on micro-patterned Si substrates [J]. Journal of Applied Physics, 2015, 118(7): 075701.

[16] Yu H P, Roberts C, Murray R. Influence of indium segregation on the emission from InGaAs/GaAs quantum wells[J]. Applied Physics Letters, 1995, 66(17): 2253-2255.

[17] Wang J, Ren X M, Deng C, et al. Extremely low-threshold

current density InGaAs/AlGaAs quantum-well lasers on silicon [J]. Journal of Lightwave Technology, 2015, 33(15): 3163-3169.
[18] Denteneer P J, de Walle C G V, Pantelides S T. Microscopic structure of the hydrogen-boron complex in crystalline silicon[J]. Physical Review B, 1989, 39(15): 10809-10824.
[19] 马明磊, 吴坚, 杨沐, 等. 基于两端自发荧光辐射的808 nm半导体激光器增益偏振特性实验表征和能带分析[J]. 物理学报, 2013, 62(17): 174209.
Ma M L, Wu J, Yang M, et al. Experimental characterization of polarization gain properties of 808 nm semiconductor laser and analysis of energy band based on amplified spontaneous emissions from double facets[J]. Acta Physica Sinica, 2013, 62(17): 174209.
[20] Kong Y T, Ma R, Shen B, et al. Experimental detection on thickness fluctuation of $In_xGa_{1-x}As$-based indium-rich cluster structure[J]. IEEE Photonics Journal, 2022, 14(6): 5858004.
[21] Matthews J W, Blakeslee A E. Defects in epitaxial multilayers I. misfit dislocations[J]. Journal of Crystal Growth, 1974, 27: 118-125.
[22] 赵天乐, 王一丁, 贾佳, 等. 半导体激光器的应用[C]//第十七届全国半导体物理学术会议. 北京: 中国物理学会, 2009: 234.
Zhao T L, Wang Y D, Jia J, et al. Application of semiconductor lasers[C]//The 17th National Academic Conference on Semiconductor Physics. Beijing: Chinese Physical Society, 2009: 234.

Polarized Dual-Peak Radiation Mechanism and Energy-Band Characteristics of InGaAs Self-Fit Well-Cluster Composite Structure

Yu Qingnan[1*], Li Ke[1], Wang Xinyu[1], Wu Jian[2], Zhang Jianwei[3], Liu Zijian[1], Xing Jiatong[1], Liao Ling[1], Ji Huixian[1], Wang Qing[1], Li Hui[1]

[1]*School of Electronic Information Engineering, Wuxi University, Wuxi* 214105, *Jiangsu, China*;
[2]*School of Physics, Beihang University, Beijing* 100191, *China*;
[3]*Changchun Institute of Optics, Fine Mechanics and Physics, Chinese Academy of Sciences, Changchun* 130033, *Jilin, China*

Abstract

Objective In this paper, a novel, highly-strained InGaAs/GaAs self-fit well-cluster composite (WCC) quantum structure was investigated. The WCC structure differs from the conventional InGaAs/GaAs quantum-well structure, which exhibits considerable potential for numerous laser applications. Presently, the conventional quantum well exhibits a quasirectangle well structure, wherein each well consists of a fixed amount of indium and a single strain type in the material system. The WCC structure with variable indium content and thickness in an $In_xGa_{1-x}As$/GaAs system can yield remarkable results, thereby facilitating the development of new laser types. This structure is associated with the indium-rich cluster (IRC) effect, wherein the IRCs were typically regarded as defects to be avoided for the conventional InGaAs quantum-well structure; hence, its special optical characteristics remain neglected. The migration of the indium atoms to the WCC structure would reduce the indium content in the corresponding InGaAs regions, consequently generating normal and indium-deficient $In_xGa_{1-x}As$ regions with hybrid strain types in the InGaAs material and aid in the production of special polarized spectra with dual peaks. Therefore, it is crucial to reveal the underlying corresponding luminescence mechanism between dual peaks in different polarized spectra and multiple $In_xGa_{1-x}As$ materials. This work offers new avenues for the development of new types of devices.

Methods First, the InGaAs-based WCC quantum structure was developed via metal-organic chemical vapor-phase deposition. To generate the IRC effect by sufficient strain accumulation, the $In_{0.17}Ga_{0.83}As$/GaAs/$GaAsP_{0.08}$ material system was designed as a periodic gain structure (Fig. 1). The thickness of the $In_{0.17}Ga_{0.83}As$ layer was designed to be 10 nm, because an InGaAs layer thinner than 10 nm is insufficient to obtain the IRC effect. Second, the luminescence mechanism of the WCC structure was studied by coating the WCC sample at a transmittance of T=99.99% at the dual facets to avoid the end reflection. Third, the polarized photoluminescence (PL) spectra in transverse electric (TE) and transverse magnetic (TM) modes were measured using a linear polarizer under varying carrier densities (N) in the range of 3.6×10^{17}–4.8×10^{17} cm^{-3}. The special bimodal feature was observed in both TE- and TM-polarized PL spectra (Fig. 2), which could be associated with the emissions from normal and indium-deficient $In_{0.12}Ga_{0.88}As$ regions with varying band gaps. To analyze the different strain types, the lattice constant $a(x)$ of the $In_xGa_{1-x}As$ material was obtained. Subsequently, the hybrid strain types in normal and indium-deficient $In_xGa_{1-x}As$ were obtained. The compressive and tensile strain occurred in the $In_{0.17}Ga_{0.83}As$ and $In_{0.12}Ga_{0.88}As$ layers, respectively. Further, according to the transition matrix element theory, the PL spectrum in TE polarization was primarily associated with the electron-hole recombination

between the first conduction (C_1) and heavy hole (HH_1) subbands, whereas that in TM polarization was associated with the electron-hole recombination between C_1 and light hole (LH_1) subbands. Moreover, in the compressively-strained $In_{0.17}Ga_{0.83}As$ layer, the HH_1 subband lies above the LH_1 subband. Conversely, the HH_1 subband lies below the LH_1 subband in the tensile-strained $In_{0.12}Ga_{0.88}As$ layer. Finally, the underlying luminescence mechanism of the polarized spectra with dual peaks was revealed according to the above analysis.

Results and Discussions The TE- and TM-polarized PL spectra (Fig. 2) reveal the special bimodal features, and they are marked using letters A and B, and C and D, which correspond to 1.27 eV and 1.33 eV and 1.35 eV and 1.31 eV, respectively. GaAs, $In_{0.17}Ga_{0.83}As$, and $In_{0.12}Ga_{0.88}As$ yield lattice constant values of 5.65325, 5.72215, and 5.7019 Å, respectively. Accordingly, the $In_{0.17}Ga_{0.83}As$ layer is subject to compressive strain such that the HH_1 subband lies above the LH_1 subband. Meanwhile, tensile strain is noted in the $In_{0.12}Ga_{0.88}As$ layer such that the HH_1 subband falls below the LH_1 subband. According to the transition matrix element theory, the main peaks, which are marked by A and C in both TE and TM spectral curves (Fig. 2), are attributed to the compressively-strained $In_{0.17}Ga_{0.83}As$ layer; the corresponding TE photon energy is less than the TM photon energy. Meanwhile, the subpeaks marked by B and D (Fig. 2) are attributed to the tensile-strained $In_{0.12}Ga_{0.88}As$ region; the corresponding TE photon energy exceeds the TM photon energy. Moreover, the characteristics of the hybrid energy band of the InGaAs self-fit WCC quantum structure are obtained (Fig. 3). For the compressively-strained $In_{0.17}Ga_{0.83}As$ layer, the energy intervals from C1 to HH_1 and LH_1 bands are 1.27 eV and 1.35 eV, which correspond to the photon energy at peaks A and C, respectively. In the case of the tensile-strained $In_{0.12}Ga_{0.88}As$ material, the energy intervals from C_1 to HH_1 and LH_1 bands are 1.33 eV and 1.31 eV, which correspond to the photon energy at peaks B and D, respectively.

Conclusions In this paper, a novel, highly-strained InGaAs/GaAs self-fit WCC quantum structure is investigated based on the IRC effect. The measured spectra in TE and TM polarizations reveal special features with dual peaks, which are attributed to the combination of different emissions produced by the normal and indium-deficient InGaAs active regions. According to the transition matrix element theory, the corresponding luminescence mechanism between the dual peaks in polarized spectra and InGaAs material with different indium content is revealed. Furthermore, the band characteristics associated with the conduction subband C_1 and valence subbands of heavy holes HH_1 and light holes LH_1 are determined to reveal the underlying luminescence mechanism. The special WCC structure demonstrates a hybrid strain distribution, which indicates the simultaneous existence of compressive and tensile strains. The results of this study can greatly enhance the performance of InGaAs-based WCC-tunable lasers.

Key words semiconductor laser; InGaAs/GaAs; indium-rich cluster; polarized dual-peak spectrum; hybrid energy band